Numerical analysis of full-scale mechanically stabilized earth (MSE) walls under strip footing load

H. Ahmadi*
Ghent University, Belgium (hamzeh.ahmadi@ugent.be)
A. Bezuijen
Ghent University, Belgium and Deltares, Delft, The Netherlands (adam.bezuijen@ugent.be)

ABSTRACT: In this study, the results of full scale physical model geogrid-reinforced MSE walls are compared with the results of numerical analysis (Plaxis 2D) under short and long-term loading conditions. The two full scale models were only different in the flexibility of facing elements (with full rigid or full flexible face). Specifics regarding the behavior of the geogrids after the compaction load and under the strip footing load are included in the study. The focus of the paper is to compare the maximum tensile forces in reinforcement layers in the experimental tests with the numerical analysis. Based on the research findings, the maximum strains in the reinforcement layers occurred in the upper layers right below the strip footing load. The maximum wall deflection for flexible facing is larger than for rigid facing and occurred at h/H=0.81 from top of the wall. By considering the apparent cohesion of a soil-geogrid composite mass in this study, there is good agreement between the test results and numerical analysis. It appears that the geogrid has two functions it works as a 'wedge tight back' and as a soil improvement.

Keywords: Full scale model tests, MSE wall, Strip footing load, Numerical analysis.

1 INTRODUCTION

In many situations, footings are located on the backfill of retaining structures (e.g. footings for bridge abutments or roads located up on the retaining structure). When a footing is constructed behind a reinforced earth wall, the maximum tensile forces on reinforcement layers will depend on any of the following factors: (1) the location of the footing with respect to the wall, (2) the type of reinforcement, (3) the number of reinforcing layers, (4) the depth below the footing to the first layer of reinforcement, (5) the spacing between reinforcing layers and (6) the dimensions of the reinforcement compared with the dimensions of the wall (Ahmadi and Hajialilue-Bonab, 2012). The behavior of reinforced earth structures has been comprehensively studied through field observations and full-scale physical model, laboratory model testing, and numerical simulation (Frankowska, 2005; Bergado and Teerawattanasuk, 2008; Hatami and Bathurst, 2005, 2006; Won and Kim, 2007). 2D numerical analysis by considering the plane strain condition for reinforced earth structures was done by Bergado et al., 1995; Karpurapu and Bathurst, 1995; Chai et al., 1997; Rowe and Ho, 1998). They analyzed the deformation and the influence of important parameters in different types of reinforced soil walls.
Estimation of soil reinforcement loads and strains in full scale tests are the key to the accurate design of internal stability of reinforced soil structures. Accurate estimation of reinforcement

loads and strains after construction and under surcharge loading will result in more accurate design of reinforced earth structures.
About the soil-geosynthetic interaction mechanism in GRS wall, Schlosser and Long (1972) proposed that the geosynthetic reinforcement can give the soil apparent cohesion and also from the Yang 1972, study the geosynthetic reinforcement can increase effective confinement of the soil. Jonathan and Pham, 2013 developed Schlosser and Long, 1972 method for calculating the soil apparent cohesion by using the empirical equation between the maximum aggregate particle sizes, d_{max} and the reference reinforcement spacing (S_{ref} = $6d_{max}$). From this method, the apparent cohesion, c_R, of a soil-geosynthetic composite will be:

$$c_R = \left(0.7^{(S_v/S_{ref})}\right) \frac{T_f}{2S_v}\sqrt{K_P} \qquad (1)$$

K_p= coefficient of passive earth pressure; T_f = tensile strength of reinforcement; S_v= vertical spacing of reinforcement and S_{ref} = reference reinforcement spacing.
However, the interaction between the reinforced soil and strip footing load, considering the apparent cohesion for soil-geosynthetic composite, is a not yet studied in these structures. In this study the behavior of the strip footing load over the backfill of reinforced earth structures not only depends on the parameters mentioned by Ahmadi and Hajialilue-Bonab (2012), but also depends on the composite manner of the soil-geosynthetic and flexibility of the facing panel. Strains measured during construction were as limited to 0.5% and for after applying the strip footing load to 2%. Consequently in this study the long and short term stiffness in small and big strain ranges were considered for the backfill construction step and also after applying the strip footing load.

2 FULL SCALE AND NUMERICAL MODELS

2.1 *Preparing the models*

In this study the full-scale laboratory test results (two mechanically stabilized earth walls with plywood and full height concrete facing) are compared with the results of numerical analysis. The instrumentation and configuration of the walls are shown in Fig. 1. Models were prepared and tested by Pachomov at Brandenburg University of Technology Cottbus-Senftenberg, see also Pachomov et al. 2007. The numerical modeling was carried out using the two dimensional finite-element program Plaxis (Brinkgreve and Vermeer, 2002). It should be noted that on both sides of the chamber were polyethylene sheets for reducing the friction between the soil and side walls. As a result the influence of the side wall friction was only small. The physical model was 4 m high and surcharge load was applied up to 300 kPa at the end of backfill construction. The numerical analysis was done with the same dimensions, boundary conditions and soil properties, facing panel and reinforcement with the full scale tests. In experimental tests the horizontal pressure was measured at different locations from the facing panel (a=0.05, 0.38, 0.71 and 1.04 m). Over the second, fifth and sixth reinforcement layer and under the center line of the strip footing pressure cells were installed in the concrete and wooden face. The backfill soil in the test condition was compacted using light and heavy vibrating plates.

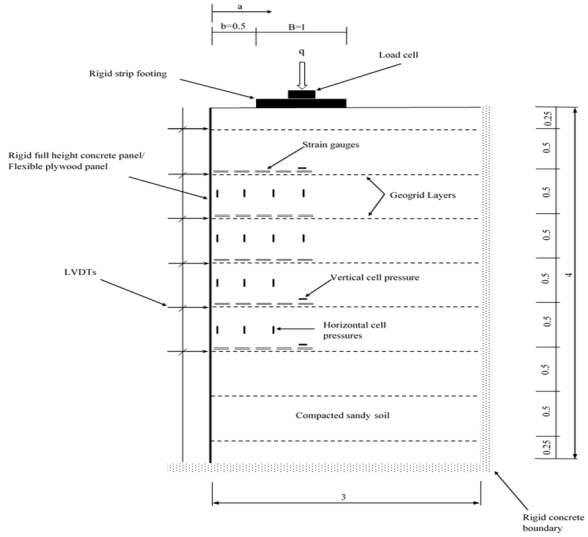

Fig. 1. Test layout for full scale models and instruments (All dimensions are in m).

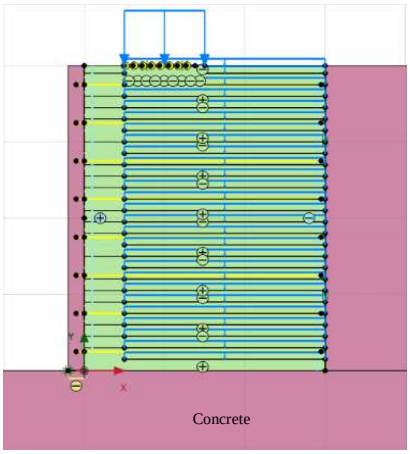

Fig. 2. Numerical model with considering the concrete material around the backfill and for the wall face.

After finishing the backfill construction also the road roller compactor was used over the backfill. The equivalent loads of the compactors used in the numerical analysis are 8, 50 and 120 kPa for light, heavy and roller compactors respectively. The strain gauges on the reinforcement layers are shown in Fig. 1. The different locations of these strain gauges were a=0.08, 0.32, 0.56, 0.8 and 1.04 m from the facing panel. Further details of the experimental and numerical models can be found in Table 1.

Fig. 2 shows the details about the rigid concrete wall in the numerical model. A Mohr-Coulomb model was applied for modeling soil behavior in numerical analysis. The geogrid reinforcement (GR) was modeled as a linear elastic material and with reinforcement-soil interface friction angle equal to the soil friction angle. Rowe and Ho, 1998 considered the perfect adherence as a reasonable assumption for the soil-geogrid interface friction coefficient ($\delta_{s,r}$=1) in numerical analysis. The plane strain condition and 15-node triangular elements with a fine mesh (3023 elements) were used for analysis. For getting more accurate results and minimizing the effect of the mesh size on the system, the mesh was refined around the reinforcement layers, strip footing and facing panel. From Jonathan and Pham, 2013 method and by considering the maximum soil particle size and first reinforcement space in the full scale test, the apparent cohesion c_R is equal to 26 kPa that used in Plaxis analysis. In this analysis, the reinforced concrete wall was assumed to be a linearly-elastic material with a modulus of elasticity of 2E7 KN/m2 and a Poisson's ratio of 0.2. This consideration helps to model correctly the base condition of the rigid wall face. Under the base of the wall, the friction angle coefficient of the rough concrete-concrete was applied by using an interface element.

A number of different strategies are available to simulate placement and compaction of soil layers. In this study a single load-unload stress cycle with a 50 kPa distributed load at the top of each backfill soil layer was used to model the compaction process. In the same method some researchers considered the compaction effect by applying a surcharge over the soil layers (Gotteland et al. 1997; Hatami and Bathurst 2005, 2006; Huang et al. 2009). For modeling the compaction effect in every new layer of backfill, a temporary uniform surcharge with 8 and 50kPa have been applied to the top surface of each backfill layer for both concrete and wooden face walls (the 8kPa uniform surcharge is only applied to the first 0.5m length of the backfill measured from the wall face). The stiffness of the GR was measured in accordance with DIN EN ISO 10319: 2008 (DIN, 2008) (ref. 6). In the Plaxis analysis, two different GR stiffness's

were considered: EA_1=680kN/m for low strains ($< 0.5\%$) and EA_2=700kN/m for high strains ($< 2\%$).

Table 1: Input parameters for Plaxis analysis.

Parameter	Symbol	Value
Wall height (m)	H	4
Unit weight-soil (kN/m3)	γ_s	17.3
Reinforcement length (m)	L	3
Vertical spacing of reinforcement (m)	Sv	0.25 and 0.5
Long term (10,000 hour) stiffness of reinforcements ($\varepsilon \leq 0.5\%$) (kN/m)	EA	670
short term (1 hour) stiffness of reinforcements ($\varepsilon \leq 2\%$) (KN/m)	EA	700
Soil Young's modulus (kN/m2)	Es	65000
Soil Poisson's ratio	ν_s	0.3
Concrete and plywood wall bending stiffness (kNm2/m)	EI	20E3, 20.25
Concrete and plywood wall normal stiffness (kN/m)	EA	6.0E6, 2.7E5
Estimated soil plane strain friction angle (Wroth 1984) (º)	φ_{ps}	44
Peak soil friction angle from the triaxial test (º)	φ_{tx}	39.09
Residual friction angle from the triaxial test (º)	φ_r	35.15
Soil dilation angle from the test (º)	ψ	12.5
Soil-reinforcement friction angle coefficient	$\delta_{s,r}$	1
Soil-concrete friction angle coefficient	$\delta_{s,c}$	0.55
Rough concrete-concrete friction angle coefficient	$\delta_{c,c}$	0.95
Soil-wood friction angle coefficient	$\delta_{s,w}$	0.45
Concrete Young's modulus (kN/m2)	E_c	2.1E8
Cohesion-soil (kPa)	C	0, 26
Unit weight-concrete (kN/m3)	γ_c	24
Concrete and wood Poisson's ratio	ν_c, ν_w	0.2, 0.33

Dilatancy angle from the sand is calculated from the test results using the relationship proposed by Schanz and Vermeer (1996):

$$sin\psi = \frac{\frac{d\varepsilon_v}{d\varepsilon_1}}{2 - \frac{d\varepsilon_v}{d\varepsilon_1}} \qquad (2)$$

The difference between triaxial and plane strain friction angles was also discussed by Wroth (1984), who proposed the linear empirical relationship:

$$8\varphi_{ps} = 9\varphi_{tx} \qquad (3)$$

2.2 *Vertical earth pressure*

Fig. 3 shows the vertical earth pressure distribution before applying the strip footing load in both the test and the Plaxis analysis. In this figure the experimental and numerical results were also compared with the vertical stress from the earth fill (γz). For the concrete face, the measurement data is located under γz-line and for the wooden face, the test data is located over the γz-line until height of 1.75m (z=2.25B). It shows that the rigidity and friction of the face can decrease the vertical earth pressure by the influence of arching effect. In this figure, there is a good agreement between the Plaxis analysis and the vertical soil pressure with γz-line distribution, but not with the experimental results when cohesion is zero (C=0 kPa). In the Plaxis analysis, for concrete and wooden face, the results are located under the γz-line when C=26kPa

and for C=0 kPa condition it's located over the γz-line. There is good agreement between the Plaxis analysis (with C=26kPa) and test results in concrete wall and also in wooden wall in shallow and deep position. However, both the test and numerical analysis results shows that the effects of vibratory compaction load on the vertical pressure in the backfill are insignificant after loading and unloading cycles. As expected, the compaction load can only increase the horizontal pressures in the numerical simulations.

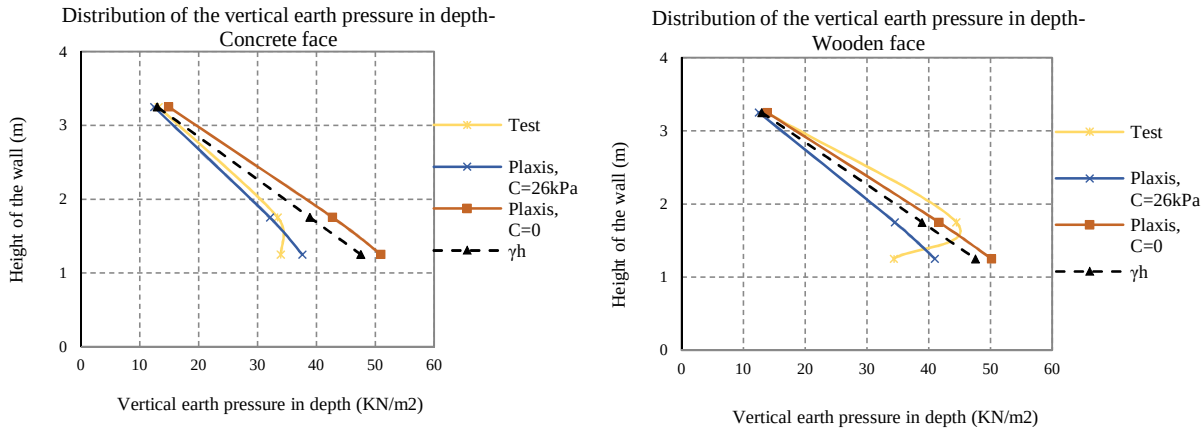

a) b)

Fig. 3. Vertical earth pressure distribution before applying the strip footing load; a) concrete face, b) wooden face

In Fig. 4, the numerical and experimental test results after applying the strip footing load (q=300 kPa) are compared with the empirical (2V:1H) method (Holtz and Kovacs, 1981).
In Fig. 4a, the test results are compared with the analytical and Plaxis analysis (C=0 and C=26kPa), the vertical earth pressure in every depth (P_v) was divided to the strip footing load applied over the backfill (q). In this figure, there is good agreement between the Plaxis analysis and test results in shallow and deep positions in concrete wall.

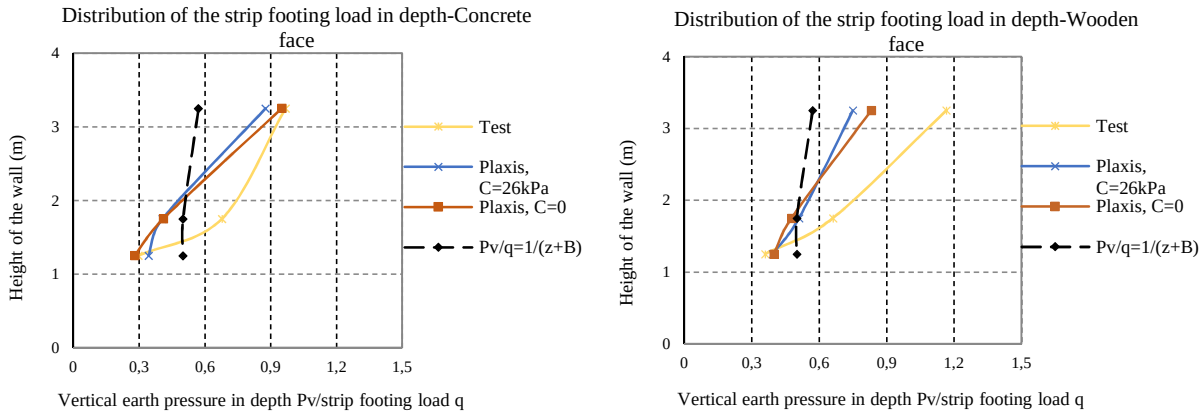

a) b)

Fig. 4. Vertical earth pressure distribution in Plaxis analysis and empirical (2V:1H) method after applying the strip footing load; a) concrete face, b) wooden face.

Also for the concrete face with q=300 kPa and for Plaxis analysis, the vertical soil pressure is smaller than the applied strip footing load (< 1) in cell pressure that located in z=0.75B.

In Fig. 4b and for the wooden face, the test and Plaxis analysis have the same pressures in depth. For z=0.75B and in test condition the pressure is more than the applied strip footing load (> 1). This can occur because of the stress concentration under the strip footing. The empirical method line (the black dashed line in the figure) for upper point, shows lower pressures than the numerical analysis and for lower points it shows higher pressures. By comparing the test data, the empirical method also shows lower pressure rather than the result in z=0.75B and 2.25B and for z=2.75B, this method has lower pressure.

2.3 *Lateral earth pressure*

In Fig. 5, the experimental and numerical results were compared with the usual analytical method under strip footing load (q=300 KN/m). The Rankine active earth pressure with a friction angle in plane strain condition ($\varphi_{ps} = 44°$) was considered. Also the empirical (2V:1H) method was applied for distribution of a strip footing load in depth (without considering the apparent cohesion). For the the concrete face as well as the wooden face the approximate method overestimates the lateral earth pressure compared with the test results and Plaxis analysis with C=26kPa, see Fig. 5a and Fig. 5b. Fig. 5a and b show that there is good agreement between the measurment and numerical analysis in determining the maximum lateral earth pressure by considering the aparant chohesion (C=26kPa). For the concrete face there are two maxima for the lateral earth pressure in test condition, one in the upper and another in the deeper position.

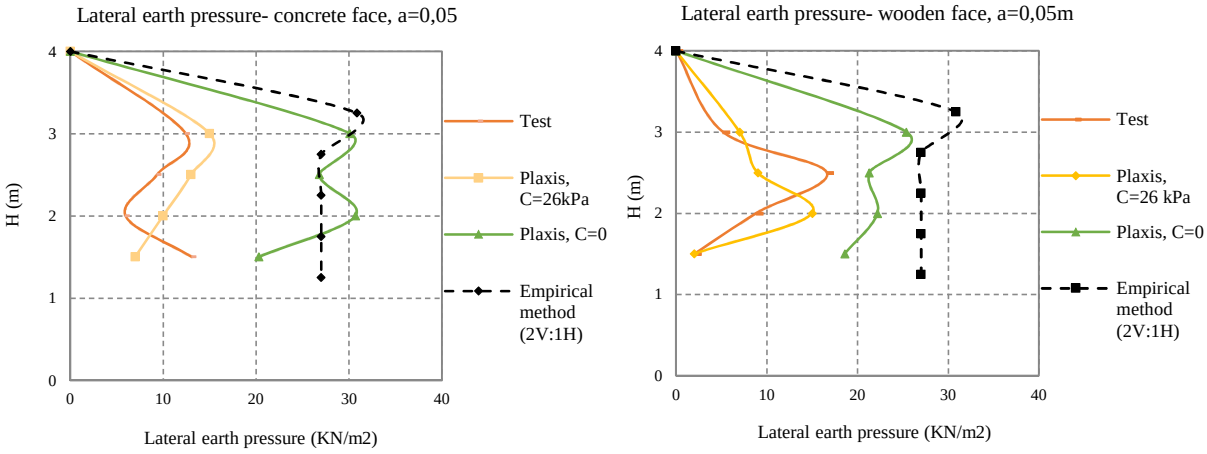

a) b)

Fig. 5. Lateral earth pressure after applying the strip footing load (300kN/m2); a) concrete face, b) wooden face.

In the wooden face a maximum in the lateral earth pressure only occurred in z=2.5m. The upper maximum in lateral earth pressure in the concrete is located at the z=3m and it shows that the failure zone for concrete face is located in shallow position rather than the wooden face.

2.4 *Lateral wall deflection*

Fig. 6a and b, show the lateral wall deflection under the strip footing load and in concrete and wooden face from the test results and Plaxis analysis. This measurement shows only the wall deflection after applying the 300kPa, strip footing load (without considering the lateral wall deflection at the end of backfill construction). For the wooden face, the maximum lateral wall deflection occurred in z/h=0.81 and the maximum wall deflection in the wooden face is more than in the concrete face. In the numerical analysis, similar to the test conditions, the wall

deflection was considered under the strip footing load. For the wooden face, the Plaxis simulation also showed a maximum wall deflection at z/h=0.81, see Fig. 6b. By comparing the numerical and test results about the maximum wall deflection, in average the calculated wall deflection is 10% larger when C=26kPa probably because of the small influence of the side-walls friction effect. But when C=0 kPa, there is (53-60) % difference between the numerical and test results.

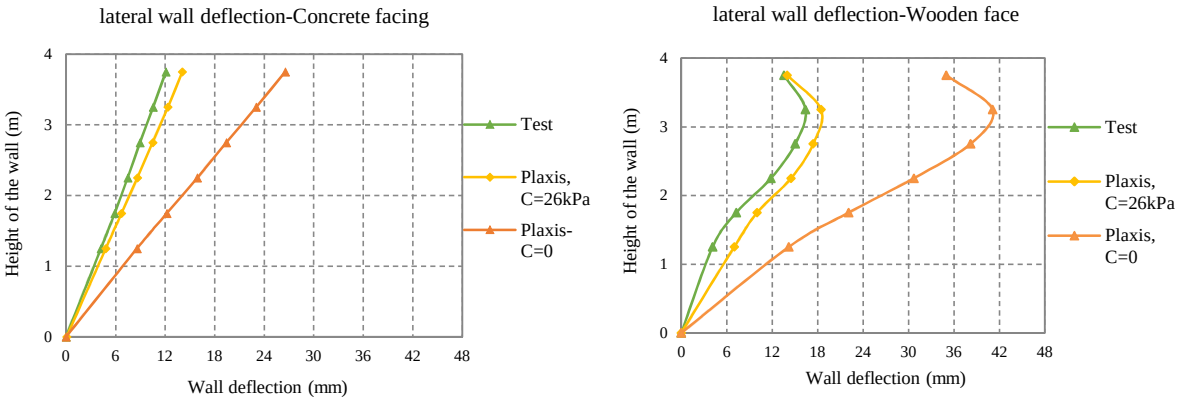

a) b)

Fig. 6. Lateral wall deflection after applying the 300 kPa, strip footing load in experimental and numerical analysis; a) concrete face, b) wooden face.

3 MAXIMUM TENSILE FORCES

Fig. 7 and Fig. 8 show the maximum tensile load on reinforcement layers from the measured and numerical analysis after applying the strip footing load in concrete and wooden face. The stiffness of the geogrid with creep effect is used for determining the maximum tensile forces in the reinforcement layers. From this figure, there is a small difference between the numerical analysis (with C=26kPa) and test results and variations of them in depth are similar to each other.

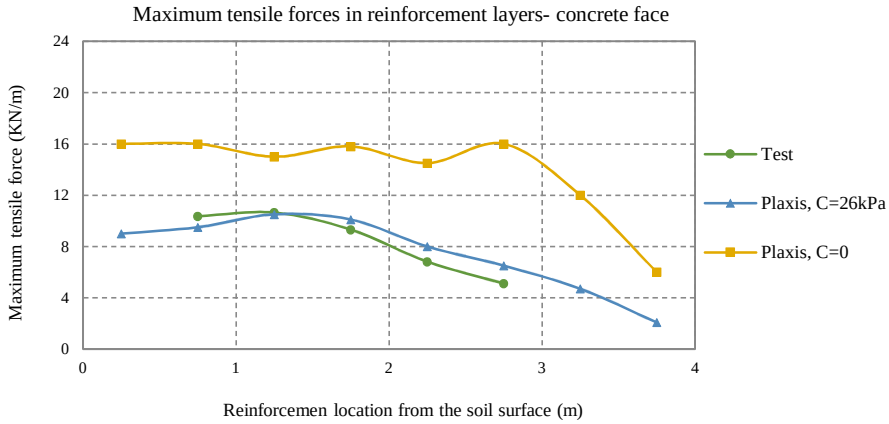

Fig. 7. Maximum tensile loads on reinforcement layers in measurement and Plaxis analysis after applying the strip footing load (300kPa); concrete face.

For concrete face, the maximum load occurred in depth of 1.75m in measurement and numerical analysis. The maximum tensile loads in the numerical analysis and test results for wooden face are larger than the stiff-face. Also in this figure there is big difference between the Plaxis analysis using C=0kPa and the test results. Indicating that the soil improvement aspect has to be taken into account in the simulations.

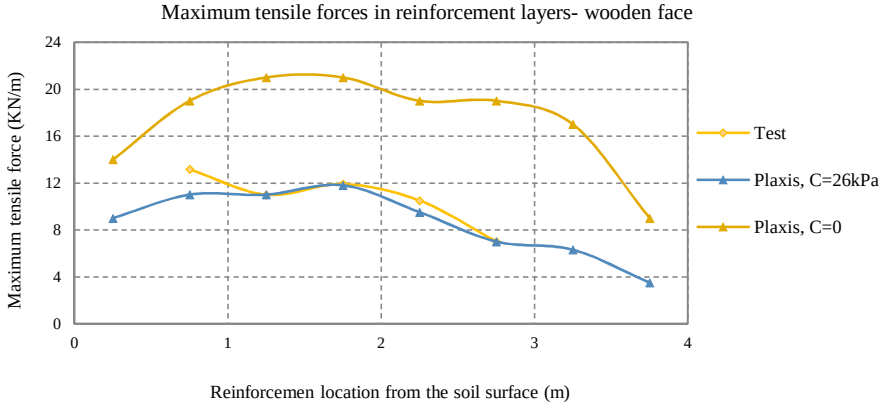

Fig. 8. Maximum tensile loads on reinforcement layers in measurement and Plaxis analysis after applying the strip footing load (300kPa); wooden face.

Table 2 presents the sum of maximum tensile forces from 2nd to 6th layer in test and Plaxis analysis. The difference between the test results and the numerical analysis is 5-6% for C=26kPa and 45.6% when C=0kPa. There is good agreement between the test results and numerical analysis in this table for wooden and conceret face by considering the aparent cohesion.

Table 2: Differences between the maximum tensile forces on reinforcement layers in test and Plaxis analysis

Models	ΣT (2nd- 6th)- Test (kN/m)	ΣT (2nd- 6th)- Plaxis-1 (kN/m)	ΣT (2nd- 6th)- Plaxis-2 (kN/m)	Differences (%)
Concrete face- after applying load	42.23	44.6	77.3	5, 45.3
Wooden face- after applying load	53.5	50.3	99	6, 45.6

4 CONCLUSIONS

Finite element analysis results with two different cohesions (C=0 and 26kPa) were compared with the experimental full-scale mechanically stabilized earth walls in this study.
It was found that the behavior of the full-scale walls was affected by the composite behavior of the soil-geogrid. By considering the apparent cohesion in the numerical analysis for the soil-geogrid interaction there is good agreement between the test and numerical results. This means that for good agreement between measurements and calculations also the soil improvement due to the geogrid has to be implemented in the simulation. When the soil improvement aspect is included in the simulation, the comparison between the maximum tensile loads in test results and the numerical analysis showed a difference between 5-6% only for after applying the strip footing load (q=300kPa). Also for wall deflection there is then 10% difference between the numerical analysis and test results.
The more rigid concrete facing panel has the maximum horizontal earth pressure on a higher point on the wall than the wooden wall. It indicates that for the flexible face after applying the

strip footing load, there is deeper failure zone than the rigid face. Also the horizontal displacements of the wall, the lateral and vertical earth pressure and the reinforcement tensile load distribution are influenced by the facing panel rigidity.

5 REFERENCES

Ahmadi H, Hajialilue-Bonab M (2012) Experimental and analytical investigations on bearing capacity of strip footing in reinforced sand backfills and flexible retaining wall. *Acta Geotech* 7(4):357–373

Bergado, D.T., Chai, J.C., Miura, N. (1995) FE analysis of grid reinforced embankment system on soft Bangkok clay. *Computers and Geotechnics* 17, 447–471.

Bergado, D.T., Teerawattanasuk, C. (2008) 2D and 3D numerical simulations of reinforced embankments on soft ground. *Geotextiles and Geomembranes* 26(1): 39-55.

Brinkgreve, R.B.J., Vermeer, P.A. (2002) Plaxis: Finite Element Code for Soil and Rock Analyses. version 8. Balkema.

Chai, J.C., Miura, N., Bergado, D.T., Long, P.V. (1997) Finite element analysis of geotextile reinforced embankment failure on soft subsoil. *Geotechnical Engineering Journal* 28 (2), 249–276.

DIN (2008). Geotextiles-Wide width tensile test (DIN EN ISO 10319:2008). Deutsches Institut für Normung e.V.

Gotteland, Ph., Gourc, J.P., Jommi, C., and Nova, R. (1996) Finite difference analysis of geotextile reinforced earth walls. *In Proceedings of EuroGeo 1*, the 1st European Geosynthetics Conference,, Maastricht, the Netherlands. pp. 503–510.

Hatami, K. and Bathurst, R.J. (2005) Development and verification of a numerical model for the analysis of geosynthetic reinforced soil segmental walls under working stress conditions. *Canadian Geotechnical Journal* 42(4): 1066-1085.

Hatami, K. and Bathurst, R.J. (2006) Numerical model for reinforced soil segmental walls under surcharge loading. *ASCE Journal of Geotechnical and Geoenvironmental Engineering* 132(6): 673-684.

Holtz, R. D. and Kovacs, W. D. (1981) An Introduction to Geotechnical Engineering, Prentice-Hall, Inc, Eaglewood Cliffs, New Jersey.

Huang, B., Bathurst, R.J. and Hatami, K. (2009) Numerical study of reinforced soil segmental walls using three different consti- tutive soil models. *ASCE Journal of Geotechnical and Geoenvironmental Engineering* 135(10): 1486-1498.

Jewell, R.A., Burd, H.J., Milligan, G.W.E. (1993) Predicting the Effect of Boundary Forces on the Behaviour of Reinforced Soil Walls. *Proceedings of the Wroth Memorial Symposium, Predictive Soil Mechanics*, Oxford, July 27-29, Thomas Telford, 378-393.

Karpurapu, R., Bathurst, R.J. (1995) Behavior of geosynthetic reinforced soil retaining walls using the finite element method. *Computers and Geotechnics* 17, 279–299.

Kazimierowicz-Frankowska, K. (2005) A case study of a geosynthetic reinforced wall with wrap-around facing. *Geotextiles and Geomembranes* 23 (1), 107–115.

Pachomov, D., Vollmert, L. and Herold, A. (2007) Der Ansatz des horizontalen Erddruckes auf die Front von KBE-Systemen Sonderheft Geotechnik, Deutsche Gesellschaft für Geotechnik e.V. DGGT, Esen, S. 129-136

Rowe, R.K. and Ho, S.K. (1998) Horizontal deformation in reinforced soil walls. *Canadian Geotechnical Journal*, Vol. 35, No. 2, pp. 312-327.

Schanz, T. and Vermeer, P. A. (1996) Angle of friction and dilatancy of sand. *Géotechnique* 46 (1), 145-151.

Schlosser, F. and Long, N. T. (1974) Recent results in French research on reinforced earth. *J. Constr. Div*., 100(3), 223–237.

Tawfiq, K.S., Caliendo, J.A. (1993) Laboratory investigation of polyethylene sheeting as a friction reducer in deep foundations. *Geotextile and Geomembranes* 12 (8), 739-762.

Won, M.S., Kim, Y.S. (2007) Internal deformation behavior of geosynthetic-reinforced soil walls. *Geotextiles and Geomembranes* 25 (1), 10-22.

Wroth, C. P. (1984) The interpretation of in situ soil tests. 24th Rankine Lecture, *Géotechnique* 34, No. 4, pp 449-489.

Wu, J. T. H. (1992) Floor discussion on long-term creep behavior, in *International Symposium on Recent Case Histories of Permanent Geosynthetic-Reinforced Soil Retaining Walls.*

Wu, J. T. H. and Helwany, S. M. B. (1996) A performance test for assessment of long-term creep behavior of soil geosynthetic composites, *Geosynthetics International*, 3(1), 1996, 107-124.

Wu, J.T.H., Pham, T., 2013. Load-carrying capacity and required reinforcement strength of closely spaced soil-geosynthetic composites. *J. Geotech. Geoenviron. Eng*. ASCE 139 (9), 1468e1476.
Yang, Z. (1972) Strength and deformation characteristics of reinforced sand. Ph.D. dissertation, Univ. of California, Los Angeles.
Yuan, Z., Swan, R. H., Jr., and Bachus, R. C. (1998) Soil confinement effect on stress-strain properties of geosynthetics, *Proceedings of the Sixth International Conference on Geosynthetics*, Atlanta, GA, pp. 523-528.